

A comparative study between Electrical Capacitance Tomography and Time-resolved X-ray tomography.

C. Rautenbach^{a,*}, R. F. Mudde^b, X. Yang^b, M. C. Melaaen^a, B. M. Halvorsen^a

^aDepartment of Process, Energy and Environmental Technology, Telemark University College, Porsgrunn, Norway.

^bKramers Laboratorium voor Fysische Technologie, Delft University of Technology, Delft, The Netherlands.

Abstract

Modern day tomographs enable the research community to investigate the internal flow behaviour of a fluidized bed by non-invasive methods that partially overcome the opaque nature of a dense bubbling bed. Each tomographic modality has its own limitations and advantages and in the present study two modern day tomographic systems were evaluated with respect to their performance on a cold dense fluidized bed. The two tomographs investigated are an Electrical Capacitance Tomography (ECT) tomograph and a time-resolved X-ray tomography tomograph. The study was performed on spherical glass particles with various particle size distributions that could mainly be classified as Geldart B or D particles. Two experimental towers were employed, one with a diameter of 10.4cm and the other 23.8cm while compressed air was used as fluidizing fluid during all of the experiments.

Results obtained with both systems are provided in comprehensive figures and tables and some first results are obtained with the time-resolved X-ray tomography system. The bubble size measurements of both tomographs are compared with several theoretical correlations via the root mean square error of the predictions (RMSEP). With the results it was also concluded that a small amount of small particles can noticeably alter the fluidization hydrodynamics of a powder. The bubble frequencies are also presented to aid in understanding the hydrodynamic behaviour of the powders investigated. A comprehensive summary of the two tomographic modalities is also provided.

Keywords: Bubble size, Fluidization, Comparative study, Electrical Capacitance Tomography (ECT), X-ray Tomography

1. Introduction

Fluidization engineering has the potential to play an important role in a sustainable future with applications in chemical looping combustion (carbon capture), recovery of valuable materials from waste streams and biomass gasification [1]. Being such a promising technology for a greener tomorrow it is important to understand these reactors with the highest possible degree of accuracy. With this aim, different measurement systems have been utilised during the history of fluidized beds [2, 3]. Positive features of fluidized beds include temperature uniformity, moderate pressure drops and the possibility of continuously adding and removing particles [1].

The main challenge faced with measuring flow behaviour in dense fluidized beds, is their opaque nature. Measurement techniques related to fluidized beds can be divided in two general categories according to Karimipour and Pugsley [4], namely: probes and photography/imaging. Probes have received criticism because they tend to interfere with the internal flow behaviour of the bed. This interference decreases with a decreasing probe size [4].

Bubbles behave differently in 2D and 3D beds according to Geldart [4] and thus 3D measurement techniques are needed. For accurate measurements, 3D information is important to fully

and accurately describe the flow behaviour (such as bubble coalescence) of the bed [4]. The development of Computational Fluid Dynamics (CFD) over the last century has aided significantly in understanding the complex flow behaviour of fluidized bed reactors but these simulations still requires verification via reliable experimental methods.

A measurement technique that is probably better known for its medical applications is the use of tomography. Some of the tomography systems (tomographs) currently available are γ -ray transmission tomography [3], Electrical Capacitance Tomography (ECT) [5], Electrical Resistance Tomography (ERT) [6], Magnetic Resonance Imaging (MRI) [7] and X-ray tomography [8]. A tomographic image (tomogram) can be generated via a variety of methods and they all produce some form of two dimensional sliced image through the investigated object. The slices can then be placed together to form a three dimensional temporal or spatial image. In Figure 1 an example is illustrated where a 3D spatial image is produced. This data were obtained using a Magnetic Resonance Imaging (MRI) system.

An example of temporal tomographic images is given in Figure 2 where several measurements taken with an Electrical Capacitance Tomography (ECT) tomograph are illustrated. These images are separated by time and if they are stacked they will form a temporal 3D image. Such images can be converted into spatial images with the use of velocity information.

Three dimensional information can also be obtain from the viewpoint of a single particle using techniques such as Positron

*T: +47 3557 5222

Email address: christo.rautenbach@hit.no (C. Rautenbach)

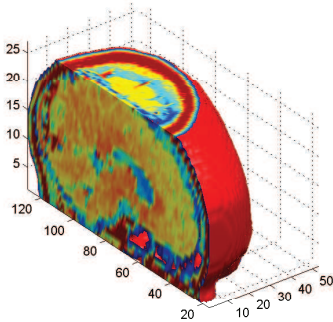


Figure 1: Spatial 3D MRI image of the human brain. This image was produced using the commercial software MATLAB and the MRI data was obtained from the MATLAB-examples data base.

Emission Particle Tracing (PEPT) systems [9, 10]. The present study will only focus on tomographs. The two tomographs investigated in the present study are the ECT and the time-resolved X-ray tomography system.

The aim of the study is to present these two tomographic modalities in such a way that researchers can make an informed choice when it comes to choosing a tomograph. The bubble size data from both tomographs are also compared to existing correlations to evaluate which correlations agree most with the obtained data.

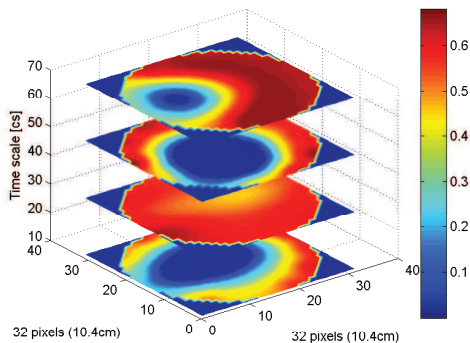


Figure 2: Four tomograms capture with a 12 electrode Electrical Capacitance Tomography (ECT) system. The images indicate a bubble rising in a gas-solid fluidized bed with the scale indicating solid fraction.

2. Overview of the ECT system

A two plane ECT tomograph was used in the present study. It consists of two arrays of electrodes, each array containing 12 electrodes. In Figure 3 a schematic drawing of the ECT sensor

is given. The location and size of the electrodes were designed by Process Tomography Ltd. [11]. As the sensor works with a soft field, it is very susceptible to external interference and thus the sensor is covered by a grounded screen to protect the electrodes from external noise. The non-intrusive design of the sensor can be observed in Figure 3. The electrodes are placed on the circumference of the 10.4cm diameter experimental tower and do not influence the flow behaviour.

The ECT tomograph produces a cross-sectional image showing the distribution of electrical permittivities of the content of the experimental tower from measurements taken at the boundary of the vessel [5]. The capacitance reading is taken between each set of electrodes and produces $E(E - 1)/2$ different readings for one image that is reconstructed. E represents the number of electrodes used in the ECT sensor [11]. These readings are interpreted and illustrated as a colourful image using a Linear Back Projection (LBP) reconstruction algorithm. An example of such an image is provided in Figure 3 via a virtual magnification of the computer screen. The resolution of the image is usually relatively low (due to soft field distortions) but can be sampled at high sample rates (low spacial resolution but high temporal resolution [2]). The quality of the image can be improved by off-line iterative LBP image reconstruction algorithms [12].

By comparing the diameter of known phantom objects with the diameter reconstructed via ECT of the same objects, McKeen and Pugsley [13] found errors between 4% and 10%, depending on the amount of iterations used in the off-line algorithm. In the present study only on-line measurements were used and the obtained data should approximately be valid as semi-quantitative results [12]. These semi-quantitative results have been confirmed by fibre optic probes in a study done by Pugsley et al. [12] by using off-line reconstruction iterations of the data collected from an 8 electrode ECT tomograph.

Both of the systems require thresholding in their obtained data. A threshold defines the void fraction that will indicate the boundary of a bubble. Each tomograph produces results using different measurements and also different reconstruction techniques. Hence each system will have a different threshold that will produce the most reliable results. In the work done by Gidaspow [20] they defined a bubble as a region where their computational simulations produced a solid fraction less than 0.2. It is a non-trivial task to decide exactly what void fraction values should be defined as a bubble as some bubbles might have a cloud surrounding it (as described by the Davidson model [21]). This cloud is associated with fast bubbles ($u_{br} > u_f = u_{mf}/\epsilon_{mf}$) and some researchers have even defined it as an independent phase since mixing across a cloud can only occur via slow molecular diffusion [20].

In another study the ECT tomograph used in the present work was utilised to measure the diameter of a standard ping-pong ball falling through the measuring planes [14]. The ball was filled with glass particles and was dropped through the empty bed. The ping-pong ball had a diameter of 2cm and after averaging the results from 7 runs and adjusting the threshold value, the ECT system measured a diameter of 2.12cm [14]. Adjusting the threshold value in the obtained data may improve

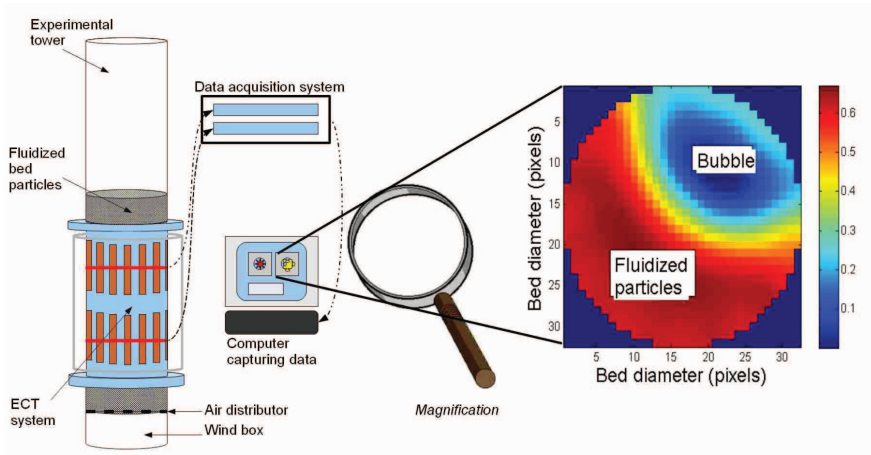


Figure 3: A schematical drawing of the 12 electrode ECT tomograph utilised in the present study together with an example of a typical cross-sectional 2D image (tomogram) obtained at a particular time instance.

the measurement accuracy of a single object passing through the ECT tomograph but will not aid in distinguishing multiple objects passing through the measuring planes. To effectively improve the measurement accuracy off-line reconstructions must be employed [12].

Nevertheless, in the present study a cylindrical hollow paperboard tube (known as a phantom object) with a diameter of 4.5cm was used to estimate the threshold value. With the threshold equal to 10% that of the unfluidized bed solid fraction the diameter of the phantom object was reconstructed with near 99% accuracy. This does however not imply that the bubble sizes will be obtained with the same degree of accuracy as the paperboard wall of the phantom object might produce distortions in the recorded permittivity values.

High-performance ECT tomographs are also being developed with a 500frame/s sample frequency with both image reconstruction and visualisation [15]. With this system direct reconstruction algorithms like the LBP, filtered LBP (FLBP) and Tikhonov regularization can be employed for on-line measurements. These images are usually blurred due to the soft field and the number of independent measurements [15]. Iterative methods are generally slow but much more accurate [15].

The obtained image consists of pixels and each represents an average solid fraction value. The average is taken over a rectangular volume equal to 1.1cm^3 [5] and is directly associated with the physical dimensions of the electrodes used in the ECT sensor. The bigger the electrodes are the bigger this averaging volume will become and the image resolution produced by the ECT system will go down. A 32×32 pixel image is produced and the pixels that fall outside the circular tower will assume zero solid fraction values (refer to Figure 2 and 3). Theoretically, the more electrodes used, the smaller the electrodes become and the more dominant the background noise can become. Thus a balance has to be kept so that the electrodes are

not too small but also not too big. The system used, with the twelve electrodes, can capture up to a hundred 32×32 matrix maps of solid fractions per second and increasing to two hundred frames per second for an 8 electrode sensor [5]. Practically between 6 and 16 electrodes are normally used [11].

This system also requires calibration. First the tower is left empty so that just air is present. The ECT software then calibrates this as the low permittivity material (the blue colour in the images used, as illustrated in Figure 2 and 3). Then the tower is filled with the particular particles and the ECT software calibrates this as the high permittivity material (the red colour in the images used as illustrated in Figure 2 and 3) [11]. This provides the reconstruction algorithm the necessary data points to represent the permittivities in-between these two extreme values.

The measuring planes are located at two different locations. One at a height of 15.65cm and the other at a height of 28.65cm above the porous plate distributor. The lower plane will be called *plane one* and the upper plane, *plane two*. Even though the ECT tomograph calculates average solid fraction values the data that are obtained are viewed as a slice through the bed at the center of each electrode. Due to the reconstruction program the measurements are also most accurate close to the center plane of the electrodes. Plane one and plane two are thus located at the center position of the electrodes (refer to Figure 3).

The two plane ECT tomograph is typically employed to measure the speed of bubbles in fluidized beds. If one bubble can be traced from one plane to the next, the time it takes for the bubble to traverse from one plane to the other, can be obtained. Using the distance between the two sensing planes the speed of a particular bubble can be determined.

Research done by Makkawi *et al* revealed that using ECT to measure dynamic parameters such as the standard deviation of the average solid fraction fluctuation and the bubble veloc-

ity or frequency, a minimum measuring span of 60s must be implemented [5]. Thus using a sampling rate of 100Hz and an experimental span of 60s, 6000 images can be produced. Up to 8000 images can be produced in one experimental span (depending on the number of electrodes, computing power and speed of the reconstruction algorithm) [5]. For the rest of this study a measuring span of 60s was implemented.

3. Overview of the time-resolved X-ray tomography system

In the X-ray measurement system used in the present study three X-ray sources were used that each created a fan beam through the fluidized bed. Each fan beam fell onto two array detector consisting of 32 CdWO₄ detectors [8]. The set-up used in the present study is illustrated in Figure 4.

The red lines represent the path of radiation detected by each detector respectively. The fluidized bed is located in the middle of the set-up, surrounded by the detectors and sources. The diameter of the bed was 23.8cm. The X-ray system can have a sampling frequency of 2500frames/s but due to some inherent noise in the X-ray sources the obtained data had to be averaged. This was done by averaging over ten measurements which in turn lowered the sampling frequency to 250frames/s. The averaged data can be converted to a line-averaged solid fraction value by using calibration curves [8].

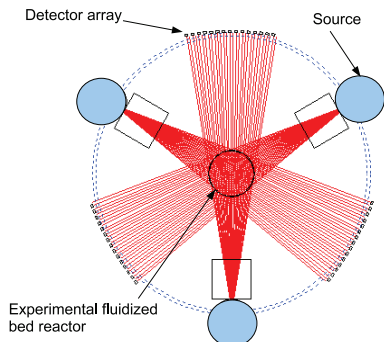


Figure 4: Three X-ray sources that simultaneously radiate an X-ray fan beam through the experimental fluidized bed tower or reactor. Two sets of 32 detectors have been allocated to each source.

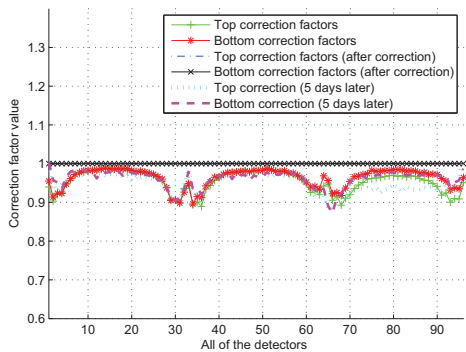
The TU Delft X-ray tomography system consists of two arrays of detectors 4cm apart and both consisting of 32 detectors for each of the 3 sources. The distance from the center of the bed to the detector arrays was 85.8cm and the distance from the center of the bed to the sources was 71.6cm. All of the X-ray beams originate from an approximate point source and diverges from there. Thus the effective distance between the measuring planes in the bed, can be shown to be equal to 1.86cm. With the two measuring planes it was possible to determine the bubble rise velocity. Bubble size and velocity are crucial in determining factor such as the particle residence time, particle entrainment and heat and mass transfer in a fluidized bed [4]. Thus to

be able to determine the bubble shape, size and velocity is important and the X-ray tomographic system allows researchers to do exactly that.

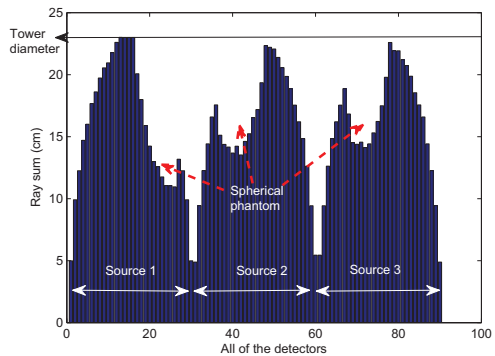
Each detector measures the attenuation of a small cone shaped beam coming from the X-ray source located on the opposite side of the fluidized bed. This small cone is approximated as a line and treated as such in the reconstruction [8]. For a mono-energetic source a two point calibration would be sufficient. This would be calibration much like that of an ECT system with an empty tower and a full tower of particles. Most X-ray sources produce a wide spectrum of X-ray energies and thus a two point calibration is not adequate [8]. This implies that the absorption coefficient is a function of the photon energy. Non-linearity is also obtained due to the fact that the low energy photons are absorbed much faster than high energy photons. Hence, R (measured number of photons) does not follow the Lambert-Beer law [8]. During calibration the effect of 'beam hardening' has to be accounted for. Beam hardening occurs as an increasing amount of powder is present on a particular X-ray beam and the relative number of high-energy photons increases [8]. To account for this effect each detector is calibrated individually with several quantities of powder. Seven calibration points are usually used in total including an empty and full tower as the two extreme values [8]. In the current study a five point calibration has been used due to the high attenuation of glass particles in comparison to that of polystyrene particles. If seven points were used, including an empty bed, the radiation would have been too low to get meaningful measurements. In the present study calibration thus entailed the center beams passing through 1/3, 1/2, 2/3, 5/6 of a full bed and a full bed. Using these calibration points the radiation level could be set high enough as to obtain meaningful measurements but also low enough as to not over expose the detector and thus avoid the detector from clipping. These criteria were chosen under the assumption that there won't be any bubbles with an effective diameter much greater than 2/3 of the tower diameter.

Before the actual measurements were made a segment of data were taken where no bubbles were present and it was then compared to the full undisturbed bed data obtained from calibration. In theory the ratio of these averaged detectors measured attenuations should be equal to 1 if the calibration is working properly. In Figure 5 (a) it is clear that this was not the case.

From Figure 5 (a) it is clear that for each of the three detector arrays a near parabolic-shaped discrepancy is obtained. This might be due to the motion of particles in the fluidized bed after fluidization and the consequent redistribution of particles. The powder used in the present study has a large range of particle sizes and thus a heterogeneous solid fraction distribution can be expected and was observed in the actual experiments. The correction factors obtained in Figure 5 (a) were used to correct all the collected data to account for these effects associated with the fluidization of the bed. These corrections were done twice to account for drift that can possibly occur within the experimental set-up. The second set of corrections were made from data captured 5 days later. In Figure 5 (a) it can be observed that one of the top detector arrays drifted the most. In Figure 5 (a)



(a)



(b)

Figure 5: (a) Two sets of correction factors calculated from data captured at separate times for all of the detectors (3×32 detectors) before and after applying the correction factor. (b) The ray-sum of the path lengths of the X-ray beams travelling through the particulate phase in a fluidized bed containing a spherical phantom.

the same ratios are also shown after it has been corrected with the correction factors and thus the drift have been accounted for in all the data collected during the current experiments.

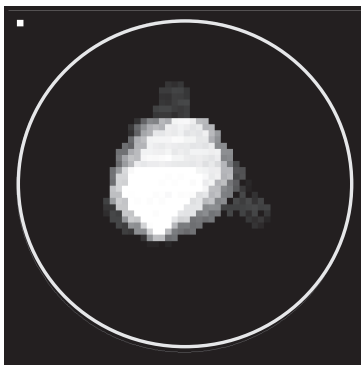


Figure 6: Typical image produced with the time-resolved X-ray tomography system illustrated in grey-scale. In the top left corner the size of a single pixel is illustrated.

A calibration curve was produced for each detector of all three double plane detector arrays. The calibration effectively produced a relationship between the measured attenuation and the distance the X-ray beam has to travel through the particulate phase. This concept is illustrated in Figure 5 (b) where the ray-sum (effective length of powder on the path of the beam) is provided for each detector. This image was created using the simulation program developed by Mudde and co-workers and simulates measurements taken with a spherical phantom (plastic rod) inserted into the bed. Each parabola represent one of the source-detector array pair and the disruption in the parabolic shape is due to the phantom. Hence the effect of a phantom or a bubble will be equivalent to having less powder in the path

of particular beams. With this path length information tomographic images can be created. For more detailed information about the calibration of a X-ray tomography system refer to work done by Mudde [8] and Rautenbach et al. [16]. In Figure 6 an example is provided of a typical time-resolved X-ray tomogram.

The images reconstructed with the time-resolved X-ray tomography system in the present study consisted of 3025 pixels (55×55 pixel image). The number of pixels used is an independent parameter and can be selected [8]. The Simultaneous Algebraic Reconstruction Technique (SART) is used that simultaneously applies the average of the corrections generated by all rays to a pixel instead of sequentially updating the pixel on a ray-by-ray basis [8]. The reconstructions are off-line, iterative and belongs to the algebraic technique class [8]. Some other reconstruction techniques that exist is the Back Projection algorithms, like those used with the ECT system, and they are significantly faster. Though these techniques are faster, they do present some limitations with regards to limited data sets [8].

A 5cm phantom object (plastic rod) was used to investigate the quantitative nature of the images produced by the system. Similar to the work done by McKeen and Pugsley [13] the actual diameter of the phantom was compared to the diameter given by the reconstructed X-ray tomograms. Errors between 6% and 25% was obtained depending on the location of the phantom. Nuclear based techniques are known for medium to high spacial resolution and the relatively high error obtained with the quantitative phantom study might be caused by the plastic walls of the phantom as the attenuation of plastic will be different to that of glass [12]. With this in mind the time-resolved X-ray tomography system should also be able to produce semi-quantitative results. In previous research done by Rautenbach et al. [16] they used the most accurate correlations, a literature study presented by S. Karimipour and T. Pugsley [4], to determine a threshold value for the presently obtained data. Therefore a threshold value of 0.465 was used for the

X-ray experiments in the present study in accordance with previous research [16].

Similar to the work done by Makkawi and Wright [5] the influence of the experimental span of time resolved X-ray tomography on the dynamic parameters in a fluidized bed was investigated by Rautenbach et al. [16]. For the time-resolved X-ray tomography system investigated, different results were obtained for various dynamic parameters. By using a single jet it was found that a measuring span of 40s produced reliable results for the bubble rise velocity. In the case of the average bubble volume and bubble frequency a 20s experiment produced reliable results when using the single jet. In using the porous plate distributor a measuring span of 45s was adequate for determining the bubble rise velocity while 25s was accurate enough for the average bubble volume and bubble frequency. In the present study an experimental span of 50s were used for all the dynamic parameters recorded with the X-ray tomography system and according to Rautenbach et al. [16] this should present reliable results when using the current X-ray system.

4. Summary of the advantages and limitations of the two tomographic modalities

These tomographic measurement system clearly hold some advantages but they also present some disadvantages or limitations (as with most measurement techniques). These strengths and weaknesses have to be considered for each particular application to find the measurement technique that is most suited for the application. For convenience these advantages and disadvantages associated with each measurement technique are summarised and presented in Table 1.

5. Experimental set-up

Glass particles with an approximate density of $2485\text{kg}/\text{m}^3$ are used in the experiments. Most of the powders utilised in the present study are classified as Geldart B or D particles. Only the powder utilised in the X-ray experiments were on the boarder between Geldart A and B and might thus exhibit characteristics from both groups. These powders all consisted of spherical particles and were chosen because of their ability to produce a bubbling bed without phenomena like spouts or channelling. Doing experiments with this 'well behaved' powders enabled the present study to focus on bubbling behaviour and illustrated the use of the two tomographic modalities without being distracted with complex phenomena like channelling.

The parameters of the two experimental set-ups are presented in Table 2 with \bar{d}_{cv} the surface-volume mean diameter, \bar{d} the arithmetic mean and u_{mf} the minimum fluidization velocity. Various particle size distributions were used during the ECT experiments. These different particle size distributions formed part of previous studies performed by Rautenbach et al. [19] and will be used in the present study to evaluate the performance of the ECT tomograph compared to that of the X-ray tomograph. The particle mixtures will be referred to as *mix 1* and *mix 2*, as indicated in Table 2. In both sets of experiments

plexiglass towers were used and compressed air at room temperature was used as fluidizing gas. The experimental tower had a diameter of 10.4cm in the ECT experiments and a diameter of 23.8cm in the time-resolved X-ray tomography experiments.

With the ECT tomograph the sensor was fixed in one location for the duration of the experiments. The sensor has two measuring planes, as depicted in Figure 3, and thus data was obtained at two distinct heights, 15.7cm and 28.7cm above the air distributor. With the time-resolved X-ray tomography tomograph measurements were taken at 24.0cm, 34.0cm and 46.2cm from the air distributor to the height where the X-ray beams left the source. This system also has 2 measuring planes but much closer together than those of the ECT tomograph and the information from these two planes are usually averaged (for example, the average bubble volume is the average of the bubble volume at the first and second plane). The averaging of the information from the two planes was not done with the ECT experiments as the sensors were too far apart.

6. Comparison between ECT and time-resolved X-ray tomography results

In Figure 7 the average bubble volume measured with the two tomographs are given as functions of the superficial velocity, u_0 . In the case of the ECT measurements bubble rise velocities could not be measured. The centers of the electrodes were 13cm apart and thus bubbles will coalesce as the bubbles traverse from one measuring plane to the next. Thus bubble velocity correlations were used to create a spatial 3D image from the collected temporal tomographic data [19].

The dependence of the minimum fluidization velocity on the particle size distribution is clearly illustrated in Figure 7. To be able to compare the results in a more direct manner Figure 8 is provided where the average bubble volume were plotted against a dimensionless coefficient (DC) expressed as

$$DC = \frac{u_0 - u_{mf}}{\sqrt{gd}}, \quad (1)$$

where g is gravitational acceleration and \bar{d} is the particular mean particle size presented in Table 2. The dimensionless coefficient takes into account most of the effects of the mean particle size and thus allows the data to be viewed together in a more comparative way. From both Figure 7 and 8 it is clear that the bubbles become larger as they move upward through the bed. Interesting result are given by the mixed particle size distributions. In Figure 7 and 8 the 100 – 200 μm powder behaves similar to the *mix 1* powder at both plane 1 and plane 2. The most interesting result is obtained with the *mix 2* powder. For the same values of the dimensionless coefficient in Figure 8, the *mix 2* powder revealed much smaller bubbles compared to the other powders. With the *mix 2* powder the measurements at plane 2 suggest that a maximum bubble size has been reached as the bubble volume does not increase monotonously. This is an interesting result as the powder can still be classified as a Geldart D powder but exhibits behaviour that is typical for Geldart A particles [21]. Thus a small amount of small particles

Table 1: Properties of the two tomographic systems investigated in the present study.

Property	ECT	Time-resolved X-ray tomography	General comments
Spatial resolution	1.79cm for the current 12 electrode system (on-line resolution without off-line processing). According to the manual it is not a trivial task to express the radial resolution mathematically but an indication of the radial resolution can be calculated using M/E . Here M is the number of independent measurement that can be made and E is the number of electrodes [11].	Approximately 2.5cm but this resolution can be improved upon if the outer detectors are shielded to allow higher energy radiation to be used. This would improve the resolution in the center of the bed without over exposing the side detectors. (Off-line data processing)	Both systems are more sensitive close to the tower walls and thus has a higher resolution close to the walls.
Size limitation	10.4cm is close to the maximum tower diameter that the ECT system can handle up to date. This limitation is due to the soft field the ECT system employs to capture solid fraction distributions.	This system has no tower size limits as it works with a hard field. With the appropriate calibration and detector installations measurements can be made in large set-ups.	The larger the experimental tower the higher energy X-rays has to be used.
Tower content (powders used)	Must be non-conductive	Material may be conductive but must not attenuate too much X-ray radiation. The denser the substance the more radiation is attenuated.	
Measurement frequency	100Hz but when working with the average solid fraction values obtained from each measurement, every 5 values are usually averaged to lower the noise.	250Hz, after a average over every 10 images has been made to lower the inherent noise associated with the X-ray source.	Due to the current reconstruction algorithm of the ECT system it can give an on-line image of the content of the tower with a frequency of 100Hz. This makes it viable for process control applications. At the present the reconstruction of X-ray tomography data is not on-line.
Invasiveness	Neither invasive nor intrusive	Neither invasive nor intrusive	Both systems does not interfere with the internal flow behaviour of the bed.

continued on next page...→

...continued from previous page.

Property	ECT	Time-resolved X-ray tomography	General comments
3D representation	It is possible to view the data in a variety of ways including 3D images and solid fraction profiles [5].	3D images and information can readily be obtained [16, 8].	
Solid fraction representation	Solid fraction maps can be recorded for each measurement taken. This makes it possible to obtain information about the solid fraction distribution within the bed at any given time. The average solid fraction value of the tower at each time step can also be calculated that can be used for statistical analyses of the bed behaviour [17, 18].	The information obtained can mainly be used to identify and illustrate bubbles and solid fraction distributions are not obtained.	
Technical skill required	System is easy to operate and does not require a high degree of technical skill.	System requires a significant amount of technical skills including nuclear safety education and training.	Both systems require additional off-line data processing (depending on the data required).
Bubble rise velocity	Can not be determined for each particular bubble as the measurement planes were too far apart. Various sensor designs can be utilised that can measure bubble rise velocity [12].	Can readily be calculated for each particular bubble.	Bubble velocities can be calculated with the ECT system used in the present study, if the bubbles does not undergo too much transformations from one measuring plane to the next.
Safety risks	Very safe and can be used in an ordinary laboratory or industrial environment without any major safety protocols.	Very safe but a safety protocol has to be followed. The system also requires to be insulated within a lead room to prevent radiation escaping into the surrounding environment. Numerous installations have to be made to make the system run safely and effectively and thus it can not readily be used in a normal laboratory or industrial environment.	

Table 2: Relevant parameters of the powders and experimental towers used in the present study.

ECT

Particle size distribution	Mean particle size (\bar{d}_{sv}) [μm]	Solid fraction (ϵ_s) [-]	Tower diameter [m]	u_{mf} [m/s]	Distributor	Geldart classification
100 – 200 μm	153	0.68	0.104	0.02	porous plate	B
400 – 600 μm	482.9	0.68	0.104	0.21	porous plate	B
750 – 1000 μm	899.15	0.67	0.104	0.45	porous plate	D
<i>mix 1: 50% 100 – 200μm</i>						
50% 400 – 600 μm	265.58	0.66	0.104	0.04	porous plate	B
<i>mix 2: 8.5% 100 – 200μm,</i>						
8.5% 400 – 600 μm ,						
83% 750 – 1000 μm	800.35	0.7	0.104	0.27	porous plate	D

Time-resolved X-ray tomography

Particle size distribution	Mean particle size (\bar{d}) [μm]	Solid fraction (ϵ_s) [-]	Tower diameter [m]	u_{mf} [m/s]	Distributor	Geldart classification
79 – 149 μm	114	0.66	0.238	0.009	porous plate	A/B

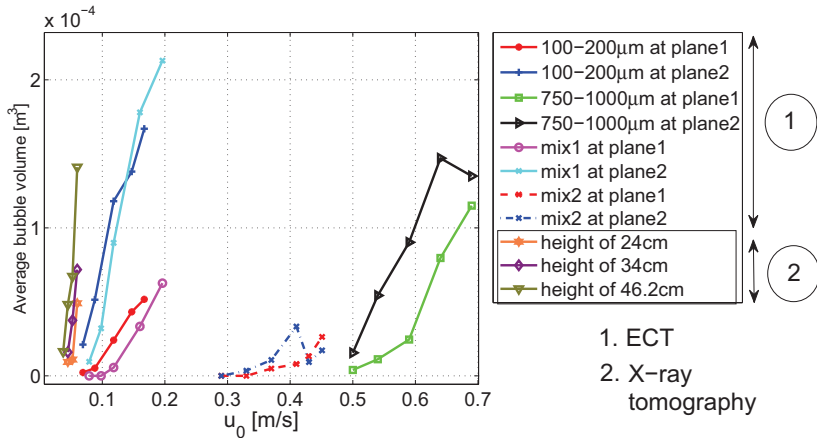


Figure 7: Comparison of the ECT- and Time resolved X-ray tomography average bubble volume data as a function of the superficial velocity, u_0 .

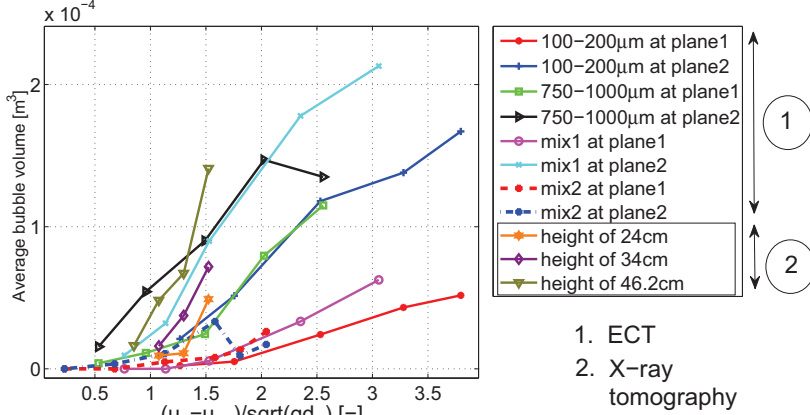


Figure 8: Comparison of the ECT- and Time resolved X-ray tomography average bubble volume data as a function of the dimensionless coefficient described in equation (1).

can change the hydrodynamic of a powder in a fluidized bed, as noted before in literature [19, 22].

The 750 – 1000 μm powder also indicates a maximum bubble volume but this is probably an indication of the onset of the slugging regime as the equivalent bubble diameter at the maximum is 63% of the tower diameter [21]. The powder used in the Time-resolved X-ray tomography experiments indicated that the bubbles kept growing as they traversed up through the bed.

In Table 3 the obtained data from both tomographs are compared to some theoretical correlations. The correlations were chosen based on the recommendation of Karimipour and Pugsley [4]. They evaluated 25 different bubble size correlations with data available from the open literature [4]. These correlations were all empirical and different measurement techniques and powders were used in creating the correlations [4]. Nevertheless they found that the correlation by Cai et al. gave the best predictions for bubble sizes especially for Geldart A and D particles [4]. The simple correlation of Mori and Wen [21] provided the best results for Geldart B particles and the correlation by Agarwal [4] provided the best correlation for measurements take with $u_0 < 10u_{mf}$. In Table 3 the condition under which each model is claimed to perform best is also provided.

In the present study the comparison between the theory and experiments will be made via the root mean square error of prediction (RMSEP) [23]. The RMSEP is a way to evaluate the prediction performance of each correlation and can be expressed as

$$RMSEP = \sqrt{\frac{\sum_{i=1}^n (\widehat{y}_i - y_i)^2}{n}}, \quad (2)$$

where \widehat{y}_i is the predicted values from the correlation, y_i is the experimental data obtained from the tomographs and n in the number of experimental data points. The RMSEP values are

given in the same unites as \widehat{y}_i and y_i . All of the correlations presented in Table 3 are expressed in centimetres and thus the comparisons were done in, and expressed in centimetres [cm].

The correlations gave predictions of the bubble size in terms of bubble diameter. To be able to compare the average bubble volume data obtained with the tomographs with the correlations, the equivalent diameters of the average bubble volumes were employed. The equivalent bubble diameter is the diameter of a sphere which will produce the same volume as a particular measured bubble.

In Table 3 it is evident that the mixed powders generally produce the largest discrepancy from the correlations especially the *mix 2* powder at plane 2. The reason for this discrepancy can be explained via Figure 7 and 8 where it is clear that the *mix 2* powder reaches a maximum bubble volume. These correlations does however not take into account all of the phenomena associated with wide particle size distributions and thus fail in accurately predicting the bubble size.

In Figure 9 the bubble frequency of each set of experiments are provided as a function of the superficial velocity. With the powders investigated with the ECT tomograph it is interesting to note that all of the powders, except the *mix 2* powder, had frequency values that increased with a low gradient at plane 2. This is a clear indication of some slugging characteristics as slugs are characterised as big periodic bubbles. All of the powders investigated with the ECT tomograph produced sharply increasing frequency values at plane 1 except the 750 – 1000 μm powder that also has a decreasing frequency at high superficial velocities (thus indicating the onset of slugs at plane 1). The *mix 2* powder was the only powder that produced sharply increasing frequency values at plane 2 that again point to the splitting and coalescence of bubbles in the powders much like a Geldart A powder. A small amount of small particles can thus be added to a slug prone powder, like the 750 – 1000 μm powder, to make the powder less prone to slugging and to lower the

Table 3: Comparison between equivalent bubble diameter data and well established correlations. The prediction performance is done via the root mean square error of prediction (RMSEP) [23].

RMSEP values for the ECT experiments [cm]				
Particle size distribution	Mori and Wen [21, 4] (Gekdart B and D)	Werther [21, 4] (Geldart A, B and D)	Agarwal [4] ($u_0 < 10u_{mf}$)	Cai et al. [4] (Geldart A and D)
Plane 1				
100 – 200 μm	0.65	0.91	0.51	0.71
750 – 1000 μm	0.64	1.33	0.39	0.88
mix 1: 50% 100 – 200 μm , 50% 400 – 600 μm .	1.77	1.88	1.39	1.64
mix 2: 8.5% 100 – 200 μm , 8.5% 400 – 600 μm , 83% 750 – 1000 μm .	2.03	2.86	1.61	1.5
Plane 2				
100 – 200 μm	0.41	1.05	1.28	0.62
750 – 1000 μm	1.33	2.39	1.02	0.65
mix 1: 50% 100 – 200 μm , 50% 400 – 600 μm .	0.76	1.41	1.48	0.97
mix 2: 8.5% 100 – 200 μm , 8.5% 400 – 600 μm , 83% 750 – 1000 μm .	3.33	4.75	2.43	2.86

RMSEP values for the Time-resolved X-ray tomography experiments [cm]				
Particle size distribution	Mori and Wen [21, 4] (Gekdart B and D)	Werther [21, 4] (Geldart A, B and D)	Agarwal [4] ($u_0 < 10u_{mf}$)	Cai et al. [4] (Geldart A and D)
Measuring plane height = 24cm				
79 – 149 μm	0.73	0.84	0.99	0.72
Measuring plane height = 34cm				
79 – 149 μm	0.79	0.92	1.02	0.59
Measuring plane height = 46.2cm				
79 – 149 μm	1.15	1.63	1.2	0.85

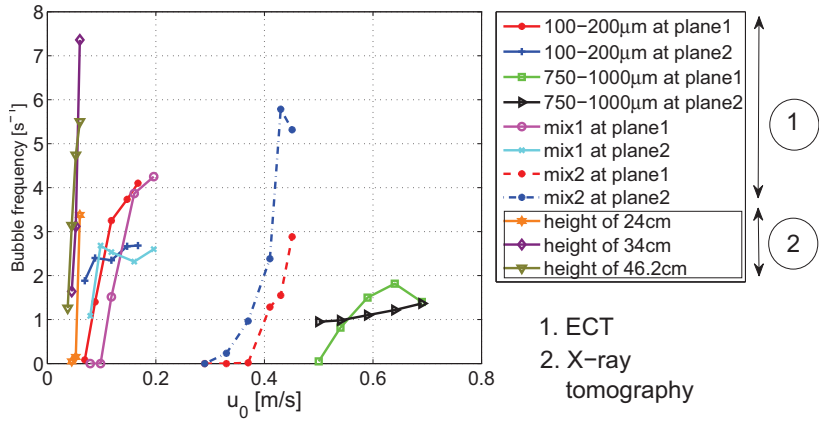


Figure 9: Bubble frequency as a function of the superficial velocity for all the experiments conducted in the present study.

minimum fluidization velocity.

The powder used in the Time resolved X-ray tomography experiments indicated that the highest frequency was observed at the second highest measuring height. The 79–149 μm powder is on the boarder between Geldart A and B particles and this high frequency at the second highest measuring plane might indicate that the bubbles split and re-coalesce in this powder as well.

7. Conclusion

The present study compared two tomographic measurement systems. The two systems used were a Electrical Capacitance Tomography (ECT) and time-resolved X-ray tomography tomograph. Both tomographs record relevant data on a non-intrusive manner and provided 3D data that could readily be employed to studying hydrodynamic effects in a fluidized bed. Each system has advantages and limitations and depending on the application a choice should be made which system is most fitting.

The results obtained from both tomographs were compared with some established bubble size correlations from the open literature. Relatively good agreement was found between the theory and experiments. The powder with the widest particle size distribution (*mix 2*) had the largest discrepancy with the theory. The conclusion was that the correlations could not account for all of the hydrodynamic effects associated with a wide particle size distribution. These conclusions were also supported by the bubble frequency data presented in the present study.

Acknowledgements

The authors like to thank Gerrit Brouwer, MSc student at the Kramers Laboratorium, Department of Multi-Scale Physics, TU Delft, for his insightful comments and helpful data analytic programs, Simen Dovland, student at Telemark University College (TUC), Porsgrunn, Norway, for his technical assistance in processing the considerable amount of experimental data. The authors thank Evert Wagner also from TU Delft for operating the time-resolved X-ray tomography system and lastly the authors thank PhD students Ru Yan and Chaminda P.G.V. Arachinge at the TUC for their assistance and technical support operating the ECT tomograph.

References

- [1] J. Grace, A perspective on development of novel fluidized bed processes for a more sustainable global future., in: S. Kim, Y. Kang, J. Lee, Y. Seo (Eds.), Fluidization XIII, ECI, South Korea, 2010, pp. 1–8.
- [2] J. R. van Ommen, R. F. Mudde, Measuring the gas-solids distribution in fluidized beds – a review, International Journal of Chemical Reactor Engineering 6 (R3) (2008) 1–29.
- [3] J. Werther, Measurement techniques in fluidized beds, Powder Technology 102 (1999) 15–36.
- [4] S. Karimipour, T. Pugsley, A critical evaluation of literature correlations for predicting bubble size and velocity in gas-solid fluidized beds, Powder Technology 205 (2011) 1–14.

- [5] Y. Makkawi, P. Wright, Electrical capacitance tomography for conventional fluidized bed measurements-remarks on the measuring technique, Powder Technology 148 (2004) 142–157.
- [6] C. Qiu, B. Hoyle, F. Podd, Engineering and application of a dual-modality process tomography system, Flow Measurement and Instrumentation 18 (2007) 247–254.
- [7] C. Muller, D. Holland, A. Sederman, M. Mantle, L. Gladden, J. Davidson, Magnetic resonance imaging of fluidized beds, Powder Technology 183 (2008) 53–62.
- [8] R. Mudde, Time-resolved x-ray tomography of a fluidized bed, Powder Technology 199 (2010) 55–59.
- [9] M. Stein, Y. Ding, J. Seville, D. Parker, Solid motion in bubbling gas fluidized beds, Chemical Engineering Science 55 (2000) 5291–5300.
- [10] X. Fan, D. Parker, Z. Yang, J. Seville, J. Baeyens, The effect of bed materials on the solid/bubble motion in a fluidized bed, Chemical Engineering Science 63 (2008) 943–950.
- [11] Process tomography Ltd., 86 Water Lane, Wilmslow, Cheshire. SK9 5BB, UK, PTL300-TP-G ECT system, Operation manual (07 2003).
- [12] T. Pugsley, H. Tanfara, S. Malcus, H. Cui, J. Chaouki, C. Winters, Verification of fluidized bed electrical capacitance tomography measurements with a fibre probe, Chemical Engineering Science 58 (2003) 3923–3934.
- [13] T. R. McKeen, T. S. Pugsley, The influence of permittivity models on the phantom images obtained from electrical capacitance tomography, Measurement Science and technology 13 (2002) 1822–1830.
- [14] R. Sharma, S. Karki, N. Masoudi, Electrical capacitance tomography for characterising bubbles in fluidized beds, Master's thesis, Telemark University College, Porsgrunn, Norway (2010).
- [15] Z. Cui, H. Wang, Z. Chen, Y. Xu, W. Yang, A high-performance digital system for electrical capacitance tomography, Measurement Science and Technology 22, 055503.
- [16] C. Rautenbach, R. Mudde, M. Melaan, B. Halvorsen, The influence of the experimental span of time-resolved x-ray tomography on the dynamic parameters in a fluidized bed., in: G. Washington, T. Jefferson (Eds.), IFSA, Industrial Fluidization South Africa, Johannesburg, South Africa, 2011.
- [17] J. Halow, G. Fasching, P. Nicoletti, J. Spenik, Observations of a fluidized bed using capacitance imaging, Chemical Engineering Science 48 (1993) 643–659.
- [18] Y. T. Makkawi, P. C. Wright, Fluidization regimes in a conventional fluidized bed characterised by means of electrical capacitance tomography, Chemical Engineering Science 57 (2002) 2411–2437.
- [19] C. Rautenbach, M. C. Melaan, B. M. Halvorsen, Investigating the influence of fines in fluidized bed reactors using 3d ect images, in: A. A. Mammoli, C. A. Brebbia (Eds.), Computational Methods in Multiphase flow VI, Wessex Institute of Technology, WIT-Press, Ashurst Lodge, Ashurst, Southampton SO40 7AA, UK, 2011, pp. 141–151.
- [20] D. Gidaspo, Multiphase Flow and Fluidization, Continuum and Kinetic Theory Descriptions, Academic Press, Harcourt Brace & Company, 525 B Street, Suite 1900, San Diego, California 92101-4495, 1994.
- [21] D. Kunii, O. Levenspiel, Fluidization Engineering, Butterworth-Heinemann, 1991.
- [22] C. van Bijlon, E. du Toit, W. Nicol, Effect of fines on the bubble properties in a two-dimensional fluidized bed by digital image analysis, in: A. Luckos, P. den Hoed (Eds.), Industrial Fluidization South Africa, Supporting sustainable strategies, Southern African Institute of Mining and Metallurgy, Chamber of Mines Building, 5 Hollard Street, Johannesburg 2017, South Africa, 2011, pp. 267–275.
- [23] K. H. Esbensen, L. P. Julius, Representative sampling, data quality, validation - a necessary trinity in chemometrics, Comprehensive Chemometrics 4 (2009) 1–20.